Lamb's Hydrostatic Adjustment for Heating of Finite Duration

TIMOTHY SOTACK AND PETER R. BANNON

Department of Meteorology, The Pennsylvania State University, University Park, Pennsylvania

(Manuscript received 24 September 1997, in final form 11 February 1998)

ABSTRACT

Lamb's hydrostatic adjustment problem for the linear response of an infinite, isothermal atmosphere to an instantaneous heating of infinite horizontal extent is generalized to include the effects of heating of finite duration. Three different time sequences of the heating are considered: a top hat, a sine, and a sine-squared heating. The transient solution indicates that heating of finite duration generates broader but weaker acoustic wave fronts. However, it is shown that the final equilibrium is the same regardless of the heating sequence provided the net heating is the same.

A Lagrangian formulation provides a simple interpretation of the adjustment. The heating generates an entropy anomaly that is initially realized completely as a pressure excess with no density perturbation. In the final state the entropy anomaly is realized as a density deficit with no pressure perturbation. Energetically the heating generates both available potential energy and available elastic energy. The former remains in the heated layer while the latter is carried off by the acoustic waves.

The wave energy generation is compared for the various heating sequences. In the instantaneous case, 28.6% of the total energy generation is carried off by waves. This fraction is the ratio of the ideal gas constant R to the specific heat at constant pressure c_p. For the heatings of finite duration considered, the amount of wave energy decreases monotonically as the heating duration increases and as the heating thickness decreases. The wave energy generation approaches zero when (i) the duration of the heating is comparable to or larger than the acoustic cutoff period, $2\pi/N_A \sim 300$ s, and (ii) the thickness of the heated layer approaches zero. The maximum wave energy occurs for a thick layer of heating of small duration and is the same as that for the instantaneous case.

The effect of a lower boundary is also considered.

1. Introduction

The prototype problem of hydrostatic adjustment was originally studied by Lamb (1932, see section 309). This one-dimensional problem considers the linear response of a stably stratified, isothermal atmosphere to an impulsive forcing located on an infinitely thin stratum of infinite horizontal extent. Lamb found that the transient response consists of dispersive acoustic-gravity waves.

Bannon (1995) has studied a generalization of Lamb's problem that involves instantaneous heating in a layer of finite thickness. Both the linear and nonlinear versions of this problem (Bannon 1995, 1996) were considered. In the linear case the transient fields responsible for the adjustment, the thermodynamic fields in the final state, and the energetics of the adjustment using Eulerian variables were described. In the nonlinear case the final fields and the energetics were described using Lagrangian variables.

Both the linear and nonlinear studies find that for an isothermal atmosphere 28.6% of the available energy generated is lost to acoustic waves. This fraction is the ratio of the ideal gas constant R to the specific heat at constant pressure c_p. However, there is an inconsistency between the results of these two cases for the partitioning of the energy between available potential energy and available elastic energy. In the linear Eulerian case both forms of energy are present in the final state; in the nonlinear Lagrangian case only available potential energy is present. The present linear study compares the Lagrangian and Eulerian descriptions. We find that the Lagrangian formulation provides a simpler, more direct explanation of the adjustment and its energetics.

The earlier work on hydrostatic adjustment used an instantaneous heating represented by a delta function in time. The delta function is mathematically convenient but physically unrealistic since heating in the atmosphere occurs over a finite period of time. Spectrally the Fourier transform of the delta function is independent of frequency. Thus instantaneous heating excites all frequencies equally. Another purpose of the present study is to examine the more general and realistic case of heating of finite duration. The transients, final state

Corresponding author address: Peter R. Bannon, Department of Meteorology, The Pennsylvania State University, 503 Walker Building, University Park, PA 16802-5013.
E-mail: bannon@ems.psu.edu

fields, and the energetics are examined for three different time sequences of the heating. Of particular interest is the effect of the duration of the heating on wave energy generation. For the case of instantaneous forcing the amount of energy deposited into the acoustic waves is large (28.6% of the total energy generated). The present study determines under what conditions more realistic heating sequences are able to produce such a large amount of wave energy. Furthermore, the effect of the thickness of the heated layer and the presence of a lower boundary is addressed.

Section 2 describes the model physics of the adjustment problem. The equations of motion are given as well as the temporal and spatial dependence of the heating. Three different time sequences of the heating are considered: a top hat, a sine, and a sine-squared heating. An equation for the vertical velocity field is presented and the method of its solution is described. Finally, the method of determining the final state is explained. Section 3 shows results for all of the heating sequences described in section 2. Unlike Bannon (1995) all of the fields are shown. These results are compared for the different heating sequences. Section 4 describes the energetics of the adjustment using both Eulerian and Lagrangian energetics. The Lagrangian energetics are shown to have a clearer interpretation than the Eulerian. The ratio of wave energy to total energy generated as a function of the thickness and duration of the heating is shown for the different heatings. Section 5 discusses the results and presents conclusions concerning the adjustment for the heating sequences considered.

2. The model

a. Governing equations

The model atmosphere is an inviscid, nonrotating, dry, diatomic ideal gas in a Cartesian coordinate system where $-g\mathbf{k}$ is the acceleration due to gravity. The isothermal base state is in hydrostatic balance and satisfies

$$\rho_0 = \rho_* \exp(-z/H_s), \qquad p_0 = p_* \exp(-z/H_s),$$
$$T_0 = T_*, \qquad \theta_0 = \theta_* \exp(\kappa z/H_s), \tag{2.1}$$

where H_s is the scale height of the atmosphere, defined by

$$H_s = \frac{RT_0}{g}; \tag{2.2}$$

κ is R/c_p, $R = 287$ J kg^{-1} K^{-1} is the ideal gas constant, and c_p and c_v are the specific heats at constant pressure and constant volume, respectively. The notation is standard: ρ, p, T, and θ are the density, pressure, temperature, and potential temperature, respectively. The nought subscript refers to the base state. An asterisk denotes a constant value. For all the numerical calculations in this study the parameter settings are $T_0 = 267$ K, $g = 9.8$ m s^{-2}, $\kappa = 2/7$, and $\gamma = c_p/c_v = 1.4$. These values yield a scale height of 7819 m.

All of the independent variables are represented as the sum of the base state and a perturbation to the base state. These one-dimensional perturbations are assumed small so that linearized equations of motion may be used. [Bannon (1996) showed that this is a good approximation for representative atmospheric heating amplitudes.] The linearized, Eulerian equations of motion describing the perturbation are

$$\rho_0 \frac{\partial w'}{\partial t} = -\frac{\partial p'}{\partial z} - \rho' g, \tag{2.3}$$

$$\frac{\partial \rho'}{\partial t} + w' \frac{d\rho_0}{dz} + \rho_0 \frac{\partial w'}{\partial z} = 0, \tag{2.4}$$

$$\frac{\partial \theta'}{\partial t} + w' \frac{d\theta_0}{dz} = \dot{\Theta}, \tag{2.5}$$

$$\frac{\theta'}{\theta_0} = \frac{p'}{\gamma p_0} - \frac{\rho'}{\rho_0}, \tag{2.6}$$

$$\frac{p'}{p_0} = \frac{T'}{T_0} + \frac{\rho'}{\rho_0}. \tag{2.7}$$

The atmosphere is perturbed by a warming of the form

$$\dot{\Theta} = \frac{\theta_0}{\rho_0 c_p T_0} Q, \tag{2.8}$$

where

$$Q = \frac{c_v}{R} \Delta p [H(z + a) - H(z - a)] F(t) \tag{2.9}$$

is the heating rate per unit volume. Here H denotes the Heaviside step function, $F(t)$ the nondimensional time dependence, and $\Delta p > 0$ a constant that gives the amplitude of the heating. For this study the half-width of the heated layer a is chosen to be 4000 m unless otherwise stated. Section 4c examines the effect of varying the half-width on the energetics. Note that $z = 0$ corresponds to the center of the heated layer and not to the location of a lower boundary.

Four different time sequences, $F(t)$, of the heating are used. The four are

$$F(t) = \begin{cases} \delta(t), & \text{delta function} \\ [H(t) - H(t - \tau)]/\tau, & \text{top hat} \\ \pi \sin\left(\dfrac{\pi t}{\tau}\right)[H(t) - H(t - \tau)]/2\tau, & \text{sine} \\ 2 \sin^2\left(\dfrac{\pi t}{\tau}\right)[H(t) - H(t - \tau)]/\tau, & \text{sine-squared.} \end{cases} \tag{2.10}$$

Here τ is the duration of the heating. Plots of those functions with a finite duration are shown in Fig. 1. All four time sequences have been normalized to produce the same net heating. The delta function case represents an instantaneous heating and was solved analytically in Bannon (1995). The top hat case represents a heating

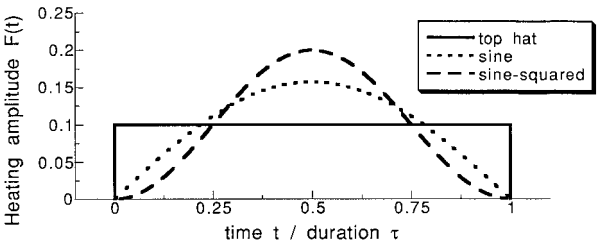

FIG. 1. Nondimensional heating amplitude, $F(t)$, as a function of time for the three heating sequences of finite duration. The duration of each sequence is τ and the integrated heating is the same for each heating sequence. The solid curve is for the top hat heating, the dashed curve is for the sine-squared heating, and the dotted curve is for the sine heating.

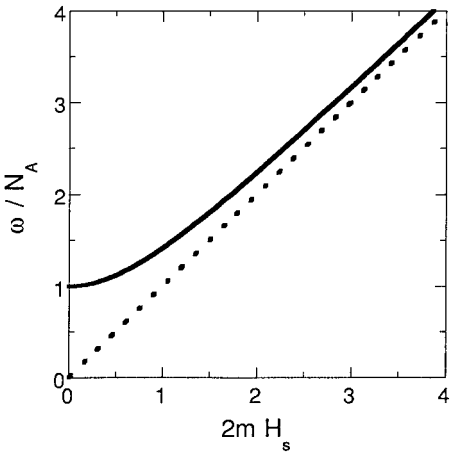

FIG. 2. The dispersion relation for the acoustic-gravity waves (solid curve) produced in the adjustment. The dashed curve corresponds to the pure acoustic case of zero gravity.

of constant strength switched on at $t = 0$ and then switched off at $t = \tau$. The sine and sine-squared heating are similarly switched on and off but they exhibit some oscillatory behavior during the period of heating. The sine-squared heating differs from the sine in that its peak is larger and its derivative vanishes at the beginning and the end of the heating.

b. *Equation for the vertical velocity and method of solution*

With the substitution,

$$w'(z, t) = e^{z/2H_s} w(z, t), \tag{2.11}$$

the equation governing the vertical velocity field is

$$\frac{\partial^2 w}{\partial t^2} + N_A^2 w - c^2 \frac{\partial^2 w}{\partial z^2} = -e^{-z/2H_s} \frac{R}{\rho_0 c_v} \frac{\partial Q}{\partial z}, \tag{2.12}$$

where $c = (\gamma R T_0)^{1/2}$ is the speed of sound and $N_A = c/2H_s$ is the acoustic cutoff frequency. For the parameter settings used, $c = 327.5$ m s^{-1} and $N_A = 2.094 \times 10^{-2}$ s^{-1} and the acoustic cutoff period $P_A = 2\pi/N_A$ is exactly 300 s.

The governing equation (2.12) is a forced hyperbolic equation that has dispersive free wave solutions. Since the atmosphere is initially at rest with $p' = \rho' = \theta' = 0$, this equation must be solved subject to the initial conditions,

$$w = 0 \quad \text{and} \quad \frac{\partial w}{\partial t} = 0 \quad \text{at } t = 0. \tag{2.13}$$

The free wave solutions of the form $w \sim \exp[i(mz - \omega t)]$ satisfy the dispersion relation

$$\omega^2 = m^2 c^2 + N_A^2. \tag{2.14}$$

A plot of the dispersion relation is shown in Fig. 2. The solid line is the dispersion relation for the waves in the presence of gravity, and the dashed line is the relation for pure acoustic waves ($g = 0$). The waves generated by the heating are acoustic waves modified by gravity. For high wavenumbers the frequency approaches that of a pure acoustic wave. These high-frequency waves do not feel the influence of gravity and act like pure acoustic waves with no dispersion. For low wavenumbers the frequency approaches the acoustic cutoff frequency, N_A. These low-frequency waves are strongly modified by gravity and are dispersive. Henceforth we refer to the high-frequency waves as the acoustic waves and the low-frequency waves as the acoustic-gravity waves.

We solve (2.12) using Laplace and Fourier transforms. The vertical velocity field in z space may be derived by taking the inverse Laplace and Fourier transforms of the equation. All of the functions (2.10) considered produce a solution that has an analytical inverse Laplace transform. Analytical inverse Fourier transforms were not found and the solution is obtained using numerical fast Fourier transform methods. Once a solution for the vertical motion field is found, the solution for the other fields may be derived using the governing equations. Solutions for each case are described in section 3.

c. *Equation for the final state*

The governing equations in their steady-state form exhibit hydrostatic degeneracy (Bannon 1995). To determine the correct state out of the infinite set of possible solutions an analog of potential vorticity must be used. The heat equation and equation of continuity may be combined to form the equation

$$\frac{\partial}{\partial t}\left[\frac{\partial}{\partial z}\left(\frac{\rho_0 \theta'}{d\theta_0/dz}\right) - \rho'\right] = \frac{1}{g}\frac{\partial Q}{\partial z}. \tag{2.15}$$

Integration of this equation with respect to time yields [using Eqs. (2.6) and (2.9) and the fact that the final state is hydrostatic] an expression for the final pressure field

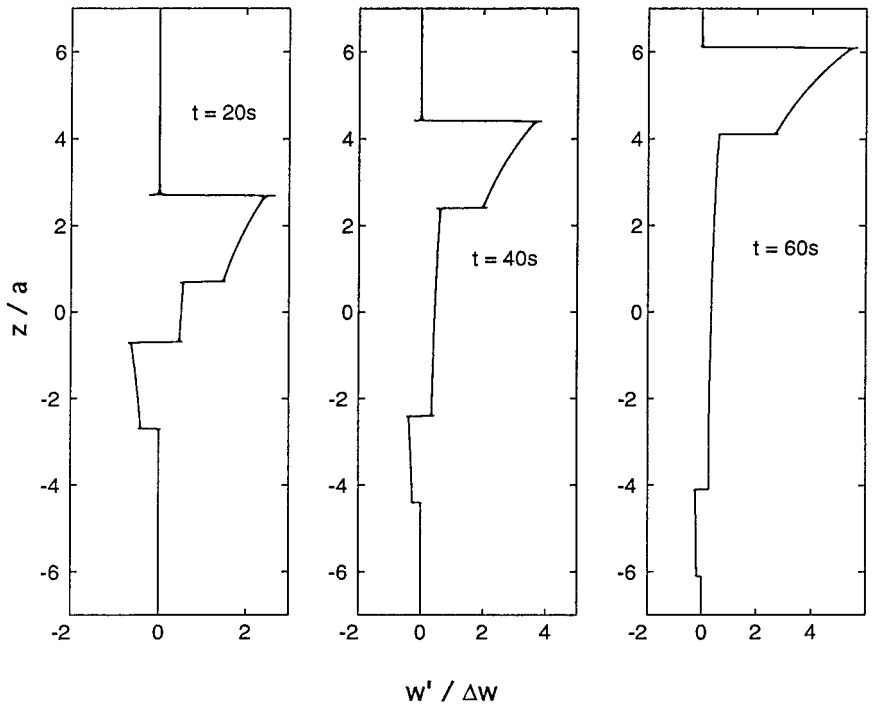

FIG. 3. Vertical velocity fields as a function of height for the case of instantaneous heating at the times $t = 20$, 40, and 60 s after the heating.

$$\frac{\partial^2 p_f'}{\partial z^2} + \frac{1}{H_s}\frac{\partial p_f'}{\partial z} = \frac{\Delta p}{\gamma H_s}[\delta(z + a) - \delta(z - a)] \int_0^\infty F(t)\, dt. \quad (2.16)$$

Since all of the heating sequences have been normalized to produce the same net heating, it follows from (2.16) that the final state fields for all of the cases will be exactly the same. Thus the final state is identical to that in Bannon (1995).

d. Boundary conditions

The atmosphere is assumed to be of infinite horizontal extent with no lateral boundaries. Most of the cases considered are for an atmosphere of infinite vertical extent, so radiation boundary conditions must be applied above and below the heated layer. In the real atmosphere, however, there is a lower boundary below the heating. For a perfectly absorbing lower boundary the solution is unchanged. For a rigid boundary the solution changes since the boundary is perfectly reflecting. The condition at a rigid boundary is that the vertical velocity must vanish there. This condition is satisfied mathematically by putting an image source of appropriate strength below the boundary at a distance equal to that from the boundary to the real source. The strength is determined by the distance of the image from the true source. We place the boundary at $z = -2a$. Then the image source is

$$Q_{\text{image}} = \frac{c_v}{R}\Delta p\{e^{3a/H_s}[H(z + 5a) - 1] - e^{a/H_s}[H(z + 3a) - 1]\}F(t). \quad (2.17)$$

This choice assures that there is no heating from the image source above the boundary and that the vertical motion field vanishes at $z = -2a$. The unequal exponential factors in (2.17) result from the presence of the exponential variation of the base state density.

3. Solutions

a. Instantaneous heating

Bannon (1995) solved the delta function case analytically for the velocity field, the final thermodynamic fields, and the energetics. The delta function case is solved in the present study using a numerical Fourier transform to test the computer code and to determine the dependence of the thermodynamic fields on time. Typically 2000 Fourier components are used. These solutions also serve to benchmark the solutions for heating of finite duration. In this section the heating halfwidth a is 4 km. Sections 3a and 3b consider an infinite atmosphere, and section 3c discusses the effect of a lower boundary on the solution.

Figure 3 shows the velocity field at three different times for the delta function case. The velocity field is scaled by $\Delta w = \Delta p/2\rho_* c$. The heating produces two significant features. One is a region of positive vertical velocity that propagates upward; the other is a region

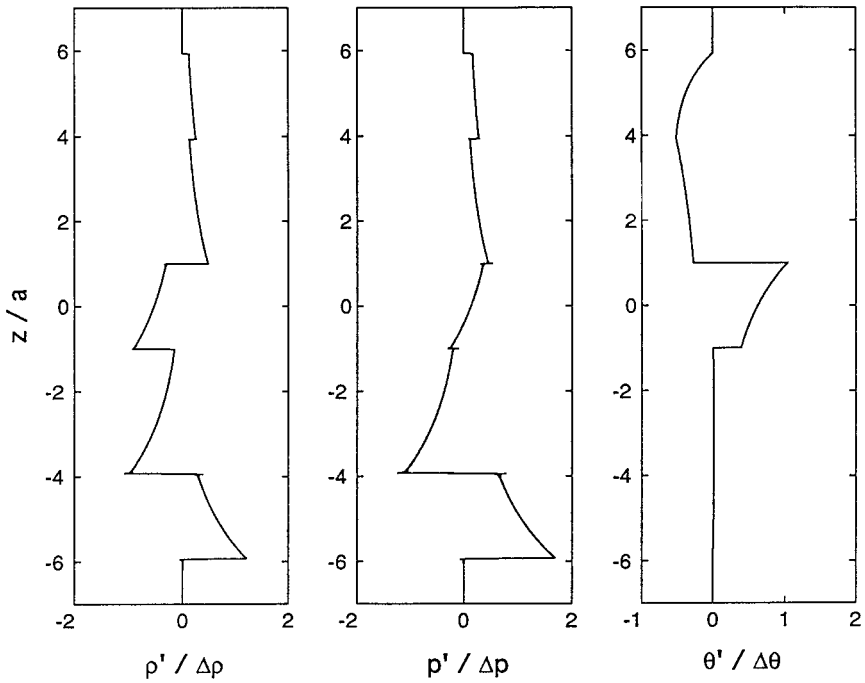

FIG. 4. Density, pressure, and potential temperature fields as a function of height for the instantaneous heating at $t = 60$ s.

of negative velocity that propagates downward. The region of positive velocity increases in amplitude as it travels upward, whereas the region of negative velocity decreases in amplitude as it travels downward. The increase/decrease is exponential and is associated with the conservation of wave energy in a medium whose density decreases exponentially with height. The wave fronts propagate away from the source region with the velocity of sound. After these acoustic wave fronts have passed, a weak trailing wake of acoustic-gravity waves follows. The slowest moving of these oscillate at the acoustic cutoff frequency, slowly decaying to zero in the final state of rest. The small tic marks evident at the edges of the wave fronts in the curves of Fig. 3 and subsequent figures arise from the use of a finite Fourier series representation of the top hat vertical structure of the heating (2.9).

Figure 4 shows a plot of the thermodynamic fields at time $t = 60$ s. The density, pressure, and potential temperature perturbations are scaled by $\Delta\rho = \Delta p/gH_s$, Δp, and $\Delta\theta = T_0\Delta p/p_*$, respectively. The plots of pressure and density show two regions of perturbation fields propagating away from the source region at the speed of sound. These features are both positive in sign and they decrease exponentially with height. This decrease is again due too the conservation of wave energy. The two fields are in phase with one another, indicating that they are essentially acoustic waves. The fields also have a significant feature present in the layer of heating ($|z| < a$). These features persist and eventually form the final fields.

The potential temperature field behaves quite differently. It has a similar feature in the layer of heating but has only one discernible feature outside this layer. This external feature lies above the heated layer and consists of a low-amplitude negative perturbation in the potential temperature field. This adiabatic cooling results from the advection of lower potential temperature air from below as the heated layer expands and raises the air above it. Below the heated layer no significant adiabatic warming or cooling is evident.

b. Heating of finite duration

The results for the vertical velocity field for the other three cases are shown in Fig. 5. Only the upper half of the domain is shown for clarity. The velocity is shown at a time of 60 s after the initiation of the heating for three different durations, $\tau = 10$, 30, and 50 s. As the duration gets closer to zero all three cases are very similar and resemble the delta function case. For larger durations, the differences between the three are more significant (Fig. 5c). As the duration increases the amplitude of the velocity decreases and the wave form broadens. The top hat produces a field that has a more distinct wave front than those of the other cases. This

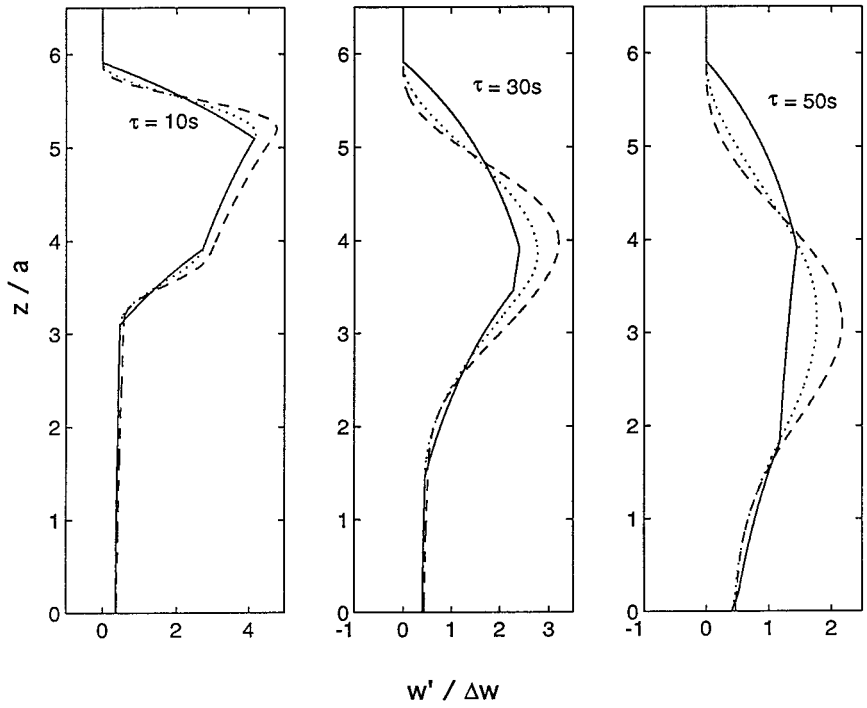

FIG. 5. Vertical velocity fields at $t = 60$ s as a function of height for the three heatings of finite duration for $\tau = 10$, 30, and 50 s. The solid curve is for the top hat heating, the dashed curve is for the sine-squared heating, and the dotted curve is for the sine heating.

behavior is expected since the top hat is a discontinuous function. The other fields, however, exhibit a larger amplitude wave form, the largest being produced by the sine-squared forcing. This amplitude relation is consistent with the peak in the forcing for each case (see Fig. 1)

The pressure and density fields for the heatings of finite duration (not shown) exhibit similar behavior as the velocity field. The wave forms for these fields are wider than those of the delta function case and have smaller amplitudes. The associated potential temperature perturbation is very similar for all three heatings of finite duration but is of smaller amplitude and broader than the delta function case. In general, the sine-squared heating produces the smoothest fields since it and its first derivative are continuous functions of time. The other heating cases are either discontinuous (the top hat case) or have a discontinuous first derivative (the sine case).

c. Effects of a lower boundary

The preceding solutions have all been for a vertically infinite atmosphere. For a rigid lower boundary, the downward propagating waves are reflected at the lower boundary and radiate upward to infinity. The reflection reverses the sign of the vertical motion but not that of the pressure field of the wave.

d. Final fields

The final pressure field may be obtained by solving the potential vorticity equation (2.16). This equation is a modified Helmholtz equation, which may be solved using the appropriate Green's function. The solution to this equation is in Bannon (1995). The density and potential temperature fields are obtained from the pressure field using the steady-state versions of equations (2.3)–(2.7). The results are the same with or without the lower rigid boundary.

Figure 6 plots the result for the density, pressure, and potential temperature fields. After the atmosphere has adjusted back to a new equilibrium in hydrostatic balance, the heated layer exhibits a reduced density but an increased pressure and potential temperature. Above the layer the potential temperature is reduced while both the density and pressure increase. This structure aloft is a consequence of vertical advection due to the upward expansion of the heated layer.

The role of advection in producing the perturbations aloft may be demonstrated using the following Lagrangian variables, denoted with a subscript L,

$$\rho'_L \equiv \rho' + \zeta' \frac{d\rho_0}{dz}, \qquad p'_L \equiv p' + \zeta' \frac{dp_0}{dz},$$

$$\theta'_L \equiv \theta' + \zeta' \frac{d\theta_0}{dz}, \qquad T'_L \equiv T' + \zeta' \frac{dT_0}{dz}, \quad (3.1)$$

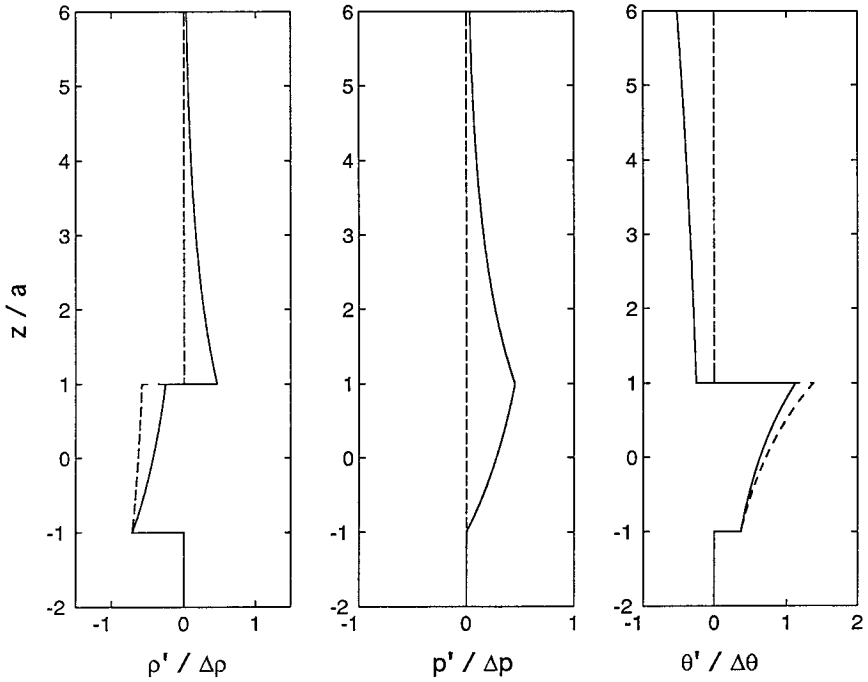

FIG. 6. Final density, pressure, and potential temperature perturbations as a function of height. The solid curves are the Eulerian variables, the dashed curves the Lagrangian variables.

where ζ' is displacement of a parcel from its initial state of rest and is related to the vertical motion field by

$$w' = \frac{\partial \zeta'}{\partial t}. \tag{3.2}$$

Figure 6 plots the Lagrangian variables (3.1) for the final state. The Lagrangian variables are nonzero only in the heated layer and vanish outside this layer. This behavior also occurs for the nonlinear problem (Bannon 1996).

Figure 6 also illustrates that below the heated layer there is no change in any of the three variables. The absence of a response in the final state below the heated layer can be explained for the case of a rigid lower boundary using a proof by contradiction. If the heated layer had, say, expanded downward during the adjustment process, then the lower fluid must have contracted and its density must have increased. However the Lagrangian potential temperature and pressure perturbation must vanish below the heated layer. The former vanishes since there is no heating there; the latter since the final pressure must be the same as the initial pressure because the mass of air aloft has not changed. Thus by Poisson's relation (2.6) the density perturbation must vanish. This feature contradicts the original assumption, thereby proving the absence of a response below the heated layer. For an infinite atmosphere the heated layer expands upward since the amount of mass aloft is finite, while that below is infinite. For either an infinite or a finite atmosphere, the absence of a final response below the heated layer holds only for a horizontally uniform heating.

4. Energetics

a. Eulerian energetics

Equations governing the energetics of the system described above can be derived from the set (2.3)–(2.7). The product of the vertical velocity and Eq. (2.3) yields an equation for the time rate of change of the kinetic energy:

$$\rho_0 \frac{\partial}{\partial t}\left(\frac{w'^2}{2}\right) = -w'\frac{\partial p'}{\partial z} - \rho' w' g. \tag{4.1}$$

This equation states that the time rate of change of the kinetic energy is equal to the rate of work done by the pressure and buoyancy forces. Similarly equations may be obtained for the available potential energy and the available elastic energy, which is the potential energy associated with the compression and expansion of a fluid. These two equations are

$$\frac{\partial}{\partial t}\left[\frac{\rho_0}{2N_0^2}\left(\frac{g\theta'}{\theta_0}\right)^2\right] = +\rho' g w' - \frac{p' w' g}{c^2} + \frac{\rho_0}{N_0^2}\left(\frac{g\theta'}{\theta_0}\right)\left(\frac{g\dot{\Theta}}{\theta_0}\right), \tag{4.2}$$

$$\frac{\partial}{\partial t}\left(\frac{p'^2}{2\gamma p_0}\right) = -p'\frac{\partial w'}{\partial z} + \frac{p' w' g}{c^2} + \frac{p'\dot{\Theta}}{\theta_0} \tag{4.3}$$

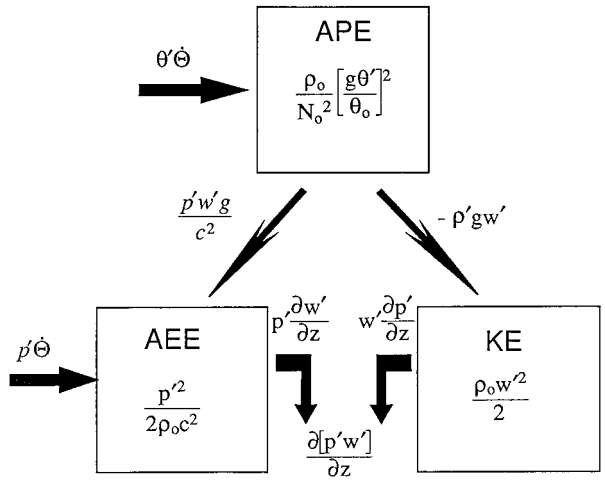

FIG. 7. Schematic diagram of the Eulerian energetics. The relationship between available elastic (AEE), available potential (APE), and kinetic energy (KE) are shown. The direction of the arrows indicates the direction of positive energy transfer.

for the available potential and elastic energies, respectively. Here $N_0^2 = (g/\theta_0)\, d\theta_0/dz$. According to (4.2) the rate of change of the available potential energy is equal to the negative of the rate of working by the buoyancy force, the generation by heating, and the conversion from available elastic energy. Equation (4.3) states that the rate of change of available elastic energy is equal to the rate of working by the pressure field, the generation due to heating, and the conversion from available potential energy. The conversion term gives the change due to the advection of higher pressure air from below. From this set it is apparent that all three of the different forms of energy are coupled together in the Eulerian representation. Their relationship is shown schematically in Fig. 7.

These equations may be combined into one equation for the rate of change of the total energy. The equation is

$$\frac{\partial}{\partial t}\left[\frac{\rho_0 w'^2}{2} + \frac{p'^2}{2\rho_0 c^2} + \frac{\rho_0}{N_0^2}\left(\frac{g\theta'}{\theta_0}\right)^2\right] = \dot{\Theta}\left[\frac{\rho_0 g^2\theta'}{\theta_0^2 N_0^2} + \frac{p'}{\theta_0}\right] - \frac{\partial(p'w')}{\partial z}. \tag{4.4}$$

The net change of the total energy is then due to the sum of the generation by heating and the rate of working by the pressure field.

From examination of the Eulerian final fields (Fig. 6) it is apparent that there is both available elastic and potential energy in the final state. However, in the Lagrangian case (Fig. 6; Bannon 1996), the final perturbation pressure is zero everywhere and there is only available potential energy in the final state. This result is consistent with the fact that there are no acoustic waves present in the final state and hence no elastic energy in the final state. The presence of available elastic energy in the final state in the Eulerian formulation arises because the pressure perturbation is defined in terms of the original base state. When the heated layer expands and comes to rest, it is in a new hydrostatic state so that there is a pressure perturbation with respect to the original state. This perturbation misleadingly implies the presence of elastic energy in the Eulerian formulation. To rectify this problem the energetics are reexamined using a Lagrangian description of the variables.

b. Lagrangian energetics

It is informative to reformulate the energetics using the Lagrangian variables (3.1). Using these new variables the equations of motion may be expressed as

$$\rho_0\frac{\partial w'}{\partial t} = -\frac{\partial p'_L}{\partial z}, \tag{4.5}$$

$$\frac{\partial \rho'_L}{\partial t} + \rho_0\frac{\partial w'}{\partial z} = 0, \tag{4.6}$$

$$\frac{\partial \theta'_L}{\partial t} = \dot{\Theta}, \tag{4.7}$$

$$\frac{\theta'_L}{\theta_0} = \frac{p'_L}{\gamma p_0} - \frac{\rho'_L}{\rho_0}. \tag{4.8}$$

The derivation of (4.5) uses the fact, obtainable from the continuity equation, that

$$\rho' + \frac{\partial(\rho_0\zeta')}{\partial z} = 0;$$

since the initial density and displacements are zero, $\rho'(t = 0) = \zeta'(t = 0) = 0$. In the Lagrangian system the convective derivatives have vanished and the buoyancy force does not appear explicitly.

In this Lagrangian system the three energy equations (4.1)–(4.3) become

$$\rho_0\frac{\partial}{\partial t}\left(\frac{w'^2}{2}\right) = -w'\frac{\partial p'_L}{\partial z}, \tag{4.9}$$

$$\frac{\partial}{\partial t}\left[\frac{\rho_0}{2N_0^2}\left(\frac{g\theta'_L}{\theta_0}\right)^2\right] = +\frac{\rho_0}{N_0^2}\left(\frac{g\theta'_L}{\theta_0}\right)\left(\frac{g\dot{\Theta}}{\theta_0}\right), \tag{4.10}$$

$$\frac{\partial}{\partial t}\left(\frac{p'^2_L}{2\gamma p_0}\right) = -p'_L\frac{\partial w'}{\partial z} + \frac{p'_L\dot{\Theta}}{\theta_0}. \tag{4.11}$$

These equations show that in the Lagrangian formulation the available potential energy is decoupled from the elastic and kinetic energies and is produced only by the heating. However the kinetic and available elastic energies remain coupled. The relationship between the different forms of energy are shown schematically in Fig. 8. The Lagrangian total energy equation is

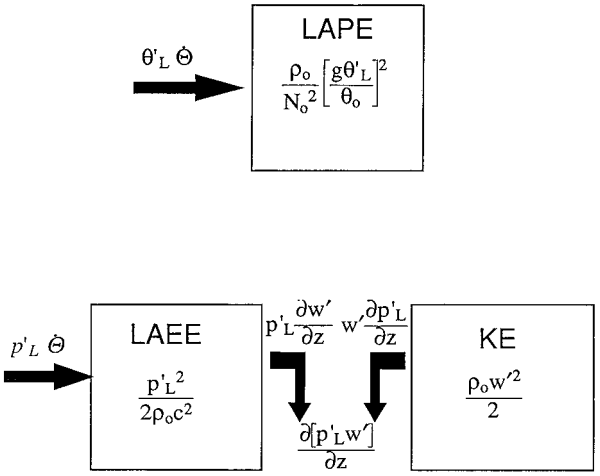

FIG. 8. Schematic representation of the Lagrangian energetics. The Lagrangian available (LAPE), Lagrangian elastic (LAEE), and kinetic energy (KE) are shown. The direction of the arrows indicates the direction of positive energy transfer.

$$\frac{\partial}{\partial t}\left[\frac{\rho_0 w'^2}{2} + \frac{p_L'^2}{2\rho_0 c^2} + \frac{\rho_0}{N_0^2}\left(\frac{g\theta_L'}{\theta_0}\right)^2\right] = \dot{\Theta}\left[\frac{\rho_0 g^2 \theta_L'}{\theta_0^2 N_0^2} + \frac{p_L'}{\theta_0}\right] - \frac{\partial (p_L' w')}{\partial z} \qquad (4.12)$$

and is isomorphic to the Eulerian result (4.4).

The linear Lagrangian formulation produces a final state (Fig. 6) in which there is no pressure perturbation ($p_L' = 0$ everywhere) and the only potential temperature perturbation is in the layer itself ($\theta_L' = 0$ above and below the layer). Thus there is no elastic energy in the final state and all of the available potential energy is located in the layer. This behavior is consistent with the nonlinear results of Bannon (1996) and with the definition of available elastic energy. Thus, the energetics is more simply described using a Lagrangian formulation.

c. *Dependence of wave energy generation on the duration and width of the heating*

The wave energy is the total generation less the energy in the final state. The amount of energy generated by the heating may be calculated from either (4.4) or (4.12) by integrating over all space and over the duration of the heating. It is straightforward to show that the energy generation in the Lagrangian formulation is equal to the energy generation in the Eulerian so that the generation may be calculated using the original Eulerian variables. The energy generation is given by

$$G = \int_0^\tau \int_{-\infty}^{\infty} \dot{\Theta}\left[\frac{\rho_0 g^2 \theta'}{\theta_0^2 N_0^2} + \frac{p'}{\theta_0}\right] dz\, dt. \qquad (4.13)$$

Since analytical expressions for the variables in physical space are unavailable, it is necessary to obtain an expression for the generation in terms of the Fourier transforms of the variables. This transformation is accomplished using Parseval's relation, which allows the integral in physical space to be evaluated as an integral in wavenumber space.

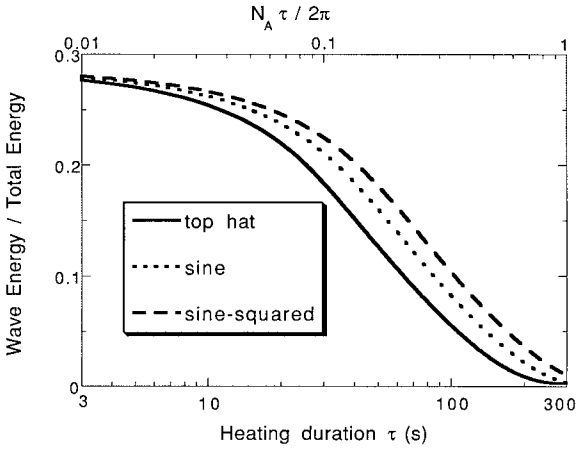

FIG. 9. Wave energy generation as a function of the heating duration τ for the three heating sequences. The wave energy is normalized by the total energy generated.

The energy generated for each of the heating sequences was calculated to determine the amount of wave energy generated for heating of finite duration. The results are shown in Fig. 9 for a heating half-width a of 4 km. The ratio of wave energy to total energy is plotted for each of the cases for heating durations τ ranging from 0 s to the acoustic cutoff period, 300 s.

The results indicate that the fraction of wave energy generated decreases with the duration of the heating for all of the cases considered. For durations less than 10 s the amount of wave energy generated is roughly the same as the delta function case for all the cases. After 10 s the fraction falls rapidly and approaches zero near the acoustic cutoff period. After 300 s almost all of the energy produced remains in the final state.

This reduction in wave energy for increasing heating duration may be explained by noting that the wave energy generation is also given by

$$\mathrm{WE} = \int_0^\tau \int_{-\infty}^{\infty} p_L' \frac{\dot{\Theta}}{\theta_0}\, dz\, dt. \qquad (4.14)$$

The generation of wave energy is dependent on the production of a Lagrangian pressure perturbation. It may be shown that this perturbation satisfies

$$\frac{1}{\gamma p_0}\frac{\partial^2 p_L'}{\partial t^2} - \frac{\partial}{\partial z}\left(\frac{1}{\rho_0}\frac{\partial p_L'}{\partial z}\right) = \frac{\partial}{\partial t}\left(\frac{\dot{\Theta}}{\theta_0}\right). \qquad (4.15)$$

The source of Lagrangian pressure perturbation is proportional to the time rate of change of the heating, so more wave energy is generated when the time rate of change is greater. Because the heating rates are nor-

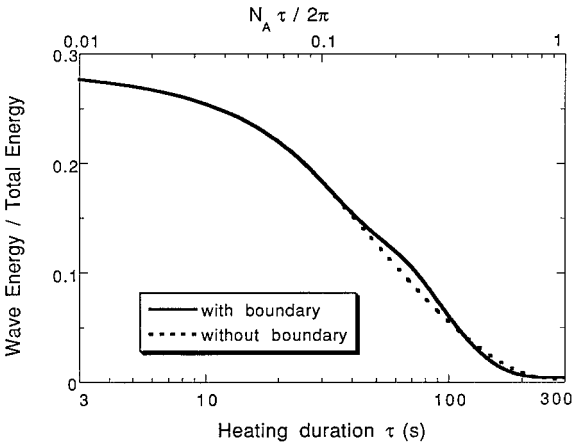

FIG. 10. Wave energy generation as a function of duration for the top hat case with and without a lower boundary at $z = -2a$. The wave energy is normalized by the total energy generated.

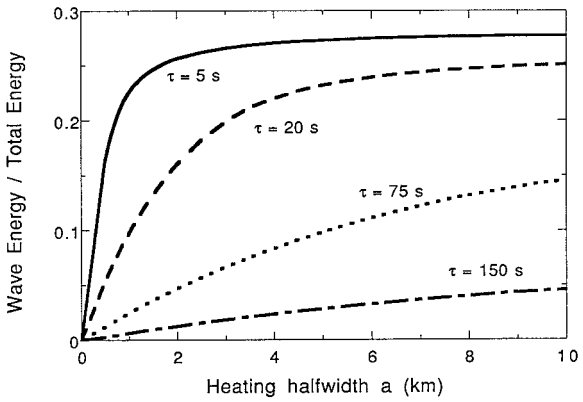

FIG. 11. Wave energy generation as a function of the heating half-width a for the top hat case for four different values of the heating duration $\tau = 5$, 20, 75, and 150 s. The wave energy is normalized by the total energy generated.

malized to produce the same net heating for different durations, heatings of smaller durations will have larger derivatives of the heating rate and will produce more wave energy.

The delta function ($\tau = 0$) case produces the greatest amount of wave energy, 28.6% of the total. The cases of finite heating duration produce less energy than this for durations greater than 10 s. The sine-squared heating, with its large temporal derivative (Fig. 1), produces the greatest amount of wave energy followed by the sine and top hat heating. The difference between the three cases can be significant. For example the wave energy for the sine-squared heating is twice that for the top hat heating when the duration is about 100 s.

Figure 10 shows the energetics of the top hat case with and without a lower boundary at $z = -2a$. Again the heating half-width a is 4 km. The lower boundary produces a small difference in the wave energy produced. The energy with a boundary oscillates about the no-boundary case with the largest increase in production for durations between 25 and 115 s and the largest decrease between 115 and 220 s. This oscillation is due to the fact that the initial pressure perturbation associated with the reflected wave is positive but becomes negative as time progresses. The timing of the onset of the oscillation is determined by the time it takes a wave to travel from the heated layer to the boundary and back. If the duration is less than this transit time then the reflected wave cannot affect the energetics. For the case displayed in Fig. 10 this time is about 25 s.

The effect of varying the half-width of the heating is displayed in Fig. 11 for the top hat heating sequence. The fraction of wave energy generated increases monotonically with the width of the heating for a fixed heating duration τ. In contrast this fraction is independent of the heating half-width and is fixed at 28.6% for an instantaneous heating. An explanation of this dependence on the heating thickness for finite duration heating follows. The wave energy generation (4.14) is the integral of the product of the Lagrangian pressure perturbation and the warming. This generation is a maximum for the instantaneous heating since the amplitude of the perturbations are greatest. For a heating of finite duration the integral is reduced since the Lagrangian pressure perturbation decreases to zero (Fig. 6) during the course of the adjustment process. A crude estimate of the adjustment time in the heated layer is given by the width of the layer divided by the sound speed,

$$\tau_{\text{adj}} \approx \frac{2a}{c}. \tag{4.16}$$

Thin layers adjust relatively quickly and their perturbations are reduced quickly, leading to a small wave energy generation. Thick layers adjust relatively slowly, leading to a large wave energy generation.

5. Conclusions

The present study considered the linear hydrostatic adjustment of an unbounded, isothermal atmosphere subjected to a horizontally uniform heating of finite duration in a layer of finite thickness. All of the heating sequences considered produced wave fronts that are broader but of smaller amplitude than that for an instantaneous heating. It was also determined that the form of the final state is unaffected by the duration of the heating provided the net heating is the same.

It was found that a Lagrangian formulation provides a simpler, more direct interpretation of the adjustment process and its energetics than an Eulerian formulation. The heating increases the potential temperature of an air parcel. Initially this entropy anomaly manifests itself as a pressure excess with no density perturbation. The heated layer then adjusts by expanding upward. The expansion and adiabatic cooling eliminates the pressure excess and the entropy anomaly then manifests itself entirely as a reduction in the air parcel's density. Since

the potential temperature is conserved in this adjustment, the Lagrangian available potential energy is unchanged while the initial available elastic energy generated is released as work done in expanding the layer and in lifting the air aloft. This interpretation is consistent with the definition of elastic energy and with the nonlinear results.

The wave energy generation was calculated as a function of the heating thickness and duration. The wave energy increases with increasing half-width with heatings of shorter duration increasing more rapidly. The fraction of wave energy generated for heatings of finite duration is less than that for the instantaneous heating. As the duration of the heating is increased the amount of wave energy produced decreases for all of the cases considered. The fraction of wave energy eventually approaches zero after the duration exceeds the acoustic cutoff period $N_A/2\pi \sim 300$ s. This reduction in wave energy is analogous to that demonstrated by Veronis and Stommel (1956) for the Rossby adjustment problem. The presence of a reflecting lower boundary has a slight impact on the wave energy generation.

The present study has limited application to the study of atmospheric convection since the heated layer is considered here to be horizontally uniform. However, Fig. 11 suggests that, regardless of the heating depth, it would be unlikely for stratiform clouds to generate substantial acoustic wave energy for characteristic heating times of several minutes. Such timescales are small compared to the lifetime of the convective systems.

Future research on the general problem of hydrostatic adjustment should consider the effects of a more realistic two- or three-dimensional heat source. For a heating of finite horizontal extent, the response of a rotating compressible fluid consists of inertia–gravity and acoustic waves that can propagate horizontally as well as vertically and the final equilibrium can have a nonzero response below the region of heating. The problem of hydrostatic and geostrophic adjustment may then be considered together.

Acknowledgments. We thank Pierre Benard and René Laprise for helpful discussion. Partial financial support was provided by the National Science Foundation under NSF Grant ATM-9521299.

REFERENCES

Bannon, P. R., 1995: Hydrostatic adjustment: Lamb's problem. *J. Atmos. Sci.*, **52,** 2302–2312.

——, 1996: Nonlinear hydrostatic adjustment. *J. Atmos. Sci.,* **53,** 3606–3617.

Lamb, H., 1932: *Hydrodynamics.* Dover, 738 pp.

Veronis, G., and H. Stommel, 1956: The action of variable wind stresses on a stratified ocean. *J. Mar. Res.,* **15,** 43–75.